JOURNAL OF APPLIED ELECTROCHEMISTRY **27** (1997) 299–307

Determination of the practical range of parameters during reverse-pulse current plating

S. ROY

Department of Chemical and Process Engineering, University of Newcastle upon Tyne, NE1 7RU, Great Britain

D. LANDOLT

Laboratoire du métallurgie chimie, Départment des matériaux, Ecole Polytechnique Fédérale du Lausanne, CH-1015, Lausanne, Switzerland

Received 2 February 1996; revised 23 May 1996

A theoretical analysis based on charge balance and steady state and transient mass-transfer considerations has been used to determine the practical range of parameters during reverse-pulse current plating. The analysis shows that small duty cycles <0.5, pulse periods in the range of 1 to 1000 ms and a dimensionless reverse-pulse current up to 2.0 define the practical regime during metal plating. This analysis has been applied to copper deposition, for which the practical domains of reverse-pulse current plating are derived. Copper is plated by reverse-pulse currents from $CuSO_4$ / H_2SO_4 solution at a rotating cylinder. The microstructure of the deposits obtained are interpreted in view of the pulse parameters and fluid hydrodynamics used.

List of symbols

a	Diffusion time parameter (s^{-1})
C	Concentration of Cu^{2+} species, (kmol m^{-3})
d	Diameter of rotating cylinder (m)
D	diffusion coefficient of Cu^{2+} species, (m^2 s^{-1})
F	Faraday's constant (96 487 C mol^{-1})
i_p	peak current (A m^{-2})
i'_p	reverse current (A m^{-2})
i^*_p	dimensionless peak current
i'^*_p	dimensionless reverse current
$i^*_{p,max}$	maximum dimensionless peak current
$i^*_{p,min}$	minimum dimensionless peak current
i_{RPL}	pulse limiting current for reverse-pulse plating
i^*_{RPL}	dimensionless pulse-limiting current
N_m	parameter for steady-state mass transfer limitation
N_p	parameter for transient mass transfer limitation
t_{on}	on time (s)
t_{rev}	reverse time (s)
T	pulse time (s)
T^*	dimensionless pulse time
z	number of electrons exchanged in a reaction

Greek letters

δ	thickness of the steady-state mass transfer boundary layer (m)
λ_m	dimensionless summation parameter
ν	kinematic viscosity (m^2 s^{-1})
θ	duty cycle (dimensionless)
Ω	cylinder rotation speed (rad s^{-1})

Superscripts and subscripts

Cu	copper
*	dimensionless
p	peak
′	reverse
m	summation index
min	minimum
max	maximum
RPL	reverse-pulse limiting

1. Introduction

Reverse-pulse current electrodeposition of metals is often used in industry to improve deposit microstructure and properties [1–7]. There have been several investigations to determine experimental reverse-pulse current parameters which yield desirable properties, such as a crack-free microstructure [8] or a uniform deposit thickness [9]. More recently, there have been attempts to eliminate bath additives by using reverse-pulse current plating [9].

Despite the continued use of the reverse-pulse current plating for such a variety of uses, there is no systematic method to fix the practical range of pulse parameters. This shortcoming not only poses a serious obstacle to the interpretation of experimental results, but also restricts the know-how needed for scale-up and intelligent operation of equipment. Some investigations have employed statistical methods to optimize pulse-parameters, for example, those necessary to achieve the highest current efficiency during hard chromium plating [10]. Although such

0021-891X

methods are helpful in planning experiments, they do not provide a rigorous basis for determining the most appropriate plating conditions.

A simple method to estimate the range of useful parameters in normal pulse plating has been presented by Chène and Landolt [11]. The evaluation of practicable parameter range for reverse-pulse plating is more difficult due to the numerous variables involved. When reverse-pulse plating is used, peak and reverse currents, pulse time and duty cycle, as well as fluid hydrodynamics can be varied independently, forming a five fold parameter space. In addition, considerations of maintaining high deposition rate and current efficiency have to be included.

In this work, a theoretical analysis is carried out to identify the parameter space where reverse-pulse current plating can be carried out. Steady state mass transfer limitations and charge balance considerations are used to fix the range of peak and reverse current densities. Transient mass transfer limitations are employed to calculate the range of pulse times and duty cycles. This analysis has been applied to copper deposition from an acid sulfate bath. Copper is plated by reverse-pulse currents from a 0.05 M or 0.1 M $CuSO_4$ and 1.0 M H_2SO_4 solution at a rotating cylinder. The microstructure of the deposits obtained in these experiments is interpreted in view of the pulse parameters and fluid hydrodynamics used. These results are compared to those obtained by pulse and direct-current plating.

2. Analysis

A typical reverse-pulse current wave form is shown in Fig. 1. The peak current, i_p, is the imposed cathodic current during the on-time, t_{on}. An anodic or reverse current, i'_p, is passed during the reverse-time, t_{rev}. The pulse period, T, is the sum of t_{on} and t_{rev}. The duty cycle, θ, is given by t_{on}/T, whereby t_{rev}/T is simply $(1-\theta)$. The four quantities, i_p, i'_p, T, and θ are called pulse parameters and can be chosen independently during reverse-current plating. In principle, more complex pulse forms are possible, for example, a reverse pulse followed by an off time. The analysis of the present paper will be restricted to pulse forms of the type shown in Fig. 1.

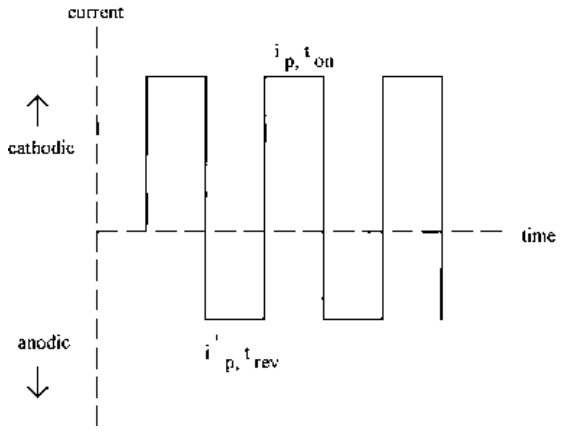

Fig. 1. A reverse-pulse current waveform.

2.1. *Charge balance and steady-state mass transfer considerations*

During reverse-pulse current deposition, the total metal plated during the on time has to exceed the metal dissolved during the reverse time for overall plating to occur. In an extreme case, when the charge reduced exactly equals the charge dissolved, no metal is plated. This fixes the minimum value of peak current which can be applied during reverse-pulse current plating for a given reverse current density. Mathematically, this relationship is expressed by

$$i_{p,\min}\ t_{on} = i'_p t_{rev} \tag{1}$$

or

$$i_{p,\min} = i'_p \frac{(1-\theta)}{\theta} \tag{2}$$

where $i_{p,\min}$ is the minimum value of peak current.

The maximum value of peak current is fixed by the condition that the maximum plating rate, averaged over an entire pulse cycle, can at most be equal to the steady state diffusion limiting current [12],

$$\frac{i_{p,\max} t_{on} - i'_p t_{rev}}{T} = i_L \tag{3}$$

where $i_{p,\max}$ is the maximum value of the peak current and i_L is the steady-state diffusion limiting current. The steady-state diffusion limiting current at a rotating cylinder is given by [13]

$$i_L = 0.0791 z_{Cu} F C_{Cu} \nu^{-0.344} d^{0.4} D^{0.644} \left(\frac{\Omega}{2}\right)^{0.7} \tag{4}$$

where C_{Cu} is the concentration of copper in the bulk electrolyte, D is the diffusivity of the Cu^{2+} species, and the other terms are as listed. Equation 3 can be rewritten as

$$i_{p,\max} = \frac{i_L T + i'_p t_{rev}}{t_{on}} \tag{5}$$

which is simply

$$i_{p,\max} = i'_p \frac{(1-\theta)}{\theta} + i_L \frac{1}{\theta} \tag{6}$$

Equations 2 and 6 define the two extreme bounds for the peak current for a given value of reverse current,

$$i'_p \frac{(1-\theta)}{\theta} \le i_p \le i'_p \frac{(1-\theta)}{\theta} + i_L \frac{1}{\theta} \tag{7}$$

Equation 7 can be normalized with respect to the steady-state diffusion limiting current, i_L, to obtain the following

$$i'^{*}_p \frac{(1-\theta)}{\theta} \le i^{*}_p \le i'^{*}_p \frac{(1-\theta)}{\theta} + \frac{1}{\theta} \tag{8}$$

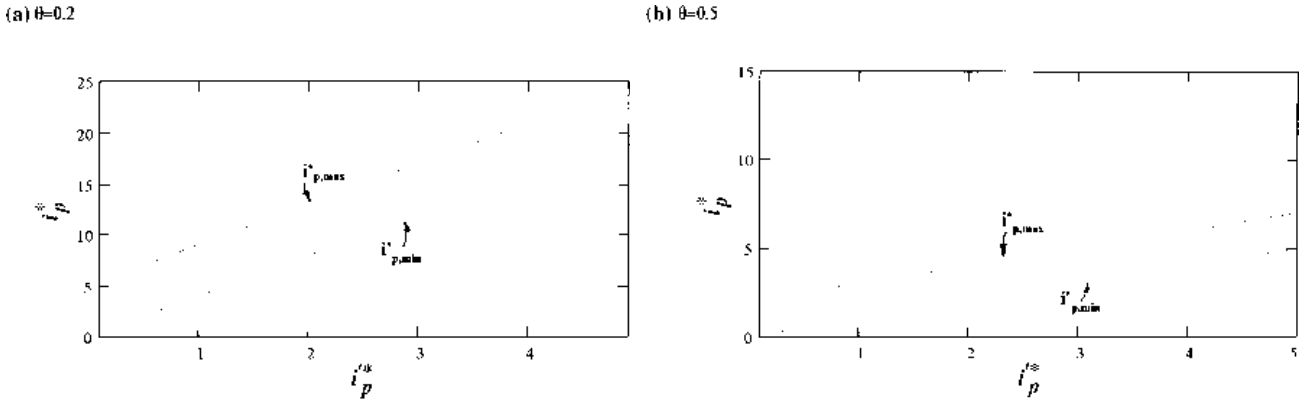

Fig. 2. Dependence of dimensionless maximum and minimum peak on reverse current: (a) $\theta = 0.2$ and (b) $\theta = 0.5$.

where i'^{*}_{p} and i^{*}_{p} are the normalized, dimensionless peak and reverse currents. Equation 8 can be further simplified as follows

$$0 < i^{*}_{p} - i'^{*}_{p}\frac{1-\theta}{\theta} < \frac{1}{\theta} \tag{9}$$

Figure 2 shows the dimensionless minimum and maximum value of peak current as a function of the dimensionless reverse-pulse current density for different duty cycles. The dimensionless peak current for metal reduction lies between the two solid lines which are the loci of the maximum and minimum peak current. When i^{*}_{p} is greater than $i^{*}_{p,max}$, competing reactions will occur at the cathode because steady-state mass transfer limitations are exceeded. If i^{*}_{P} is less than $i^{*}_{p,min}$, overall dissolution will take place. It is important to note that the minimum and maximum values of peak current are dependent solely on the duty cycle. They are independent of pulse period since only steady-state mass transfer considerations are used to fix the two limits.

The difference between the maximum and minimum peak currents is a constant, $1/\theta$. This means that when a low value of duty cycle is used, the difference between the two extremes of peak current is greater. For example, in Fig. 2, for a given value of dimensionless reverse current of 1.0, the maximum value of the dimensionless peak current is 10.0 when $\theta = 0.2$, whereas it is only 3.0 when $\theta = 0.5$. In order to attain high instantaneous peak-currents, therefore, wave-forms with small duty cycles are necessary.

2.2. *Nonsteady-state mass transfer limitations*

Although it is desirable to operate as close to the value of $i^{*}_{p,max}$ as possible, it is difficult to achieve due to transient mass transfer limitations. The maximum peak current for metal reduction during reverse-pulse current deposition is the reverse pulse limiting current density, i_{RPL}, which is given by

$$i_{RPL} = i_{L}\frac{1.0 + 2i'^{*}_{p}T^{*}\sum_{m=1}^{\infty}\frac{\exp\{\lambda_m(1-\theta)\}-1}{\lambda_m[\exp(\lambda_m)-1]}}{1.0 - 2T^{*}\sum_{m=1}^{\infty}\frac{\exp\{\lambda_m(1-\theta)\}-1}{\lambda_m[\exp(\lambda_m)-1]}} \tag{10}$$

where $T^{*} = DT/\delta^{2}$, the dimensionless pulse period, δ is the thickness of the steady-state diffusion layer, and $\lambda_m = \pi^{2}T^{*}(m\text{-}1/2)^{2}$. Equation 10 is equivalent to those existing in literature [12, 14] as is shown in the Appendix. When the applied peak current exceeds i_{RPL}, competing reactions, such as hydrogen evolution, take place, which lower the current efficiency.

Figure 3 shows the dimensionless reverse-pulse limiting current (normalized with respect to i_{L}), calculated from Equation 10, as a function of i'^{*}_{p} for different pulse periods. Values of i^{*}_{RPL} are identical to $i^{*}_{p,max}$ only for $T^{*} = 0.0001$ (i.e., very small pulse

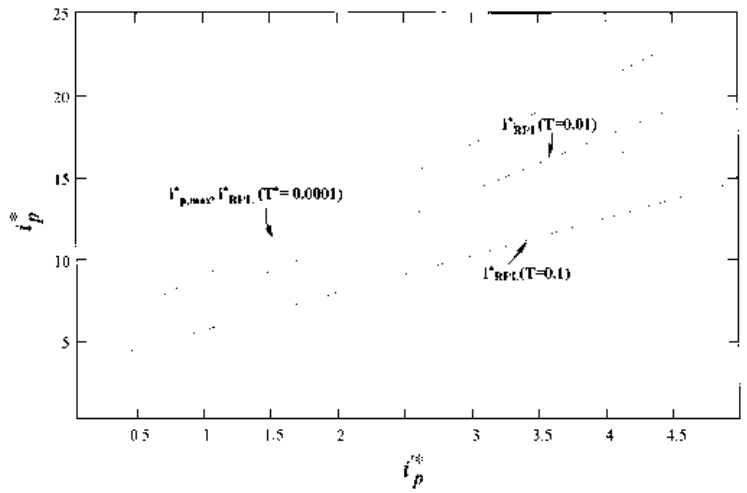

Fig. 3. The dimensionless transient mass transfer limiting current as a function of the dimensionless reverse-current density for different values of T^{*}. Duty cycle $\theta = 0.2$. (——) i^{*}_{RPL} and (·····) $i^{*}_{p,min}$.

periods) For a typical liquid-phase diffusion coefficient of 5×10^{-10} m^2 s^{-1} and a mass-transfer boundary layer thickness 2.2×10^{-5} m, such small values of T^* are possible only for pulse periods shorter than 0.1 ms, where double-layer charging currents are significant. For longer pulse periods, the reverse-pulse limiting current is always lower than $i^*_{p,max}$. For a pulse period of 10 ms the value of $T^* = 0.01$, where the values of i^*_{RPL} are significantly lower than $i^*_{p,max}$. In practice, therefore, i_{RPL} is usually lower than $i_{p,max}$ which means that transient mass transfer limitations are exceeded before those imposed by steady-state conditions.

2.3. *Parameter space in pulse and reverse pulse-plating*

For pulse plating of copper involving only cathodic pulses Chène and Landolt [11] defined a useful parameter space in terms of two dimensionless numbers N_m and N_p representing steady state and transient mass transfer limitations: $N_p = i_m/i_L$ and $N_m = i_p/i_{pL}$ where i_{pL} is the pulse limiting current density. The analysis of Chène and Landolt showed that under all conditions $N_p > N_m$ applies. Only when $N_p \leq 1$, compact deposits can be obtained with 100% current efficiency. For $N_p > 1$, the transient diffusion limitations are exceeded and dendritic deposits are obtained with a current efficiency of less than 100%.

A similar analysis can be applied to reverse-pulse current plating. The steady-state mass transfer number, N_m, is now defined as

$$N_m = i^*_p\theta - i'^*_p(1-\theta) \tag{11}$$

The transient mass transfer number is

$$N_p = \frac{i^*_p}{i^*_{RPL}} \tag{12}$$

where i^*_{RPL} is obtained from Equation 10. Different regions defined by the parameters N_m and N_p are indicated schematically in Fig. 4 and the current efficiency in these regions are presented in Table 1. The present analysis shows that there are parallels with

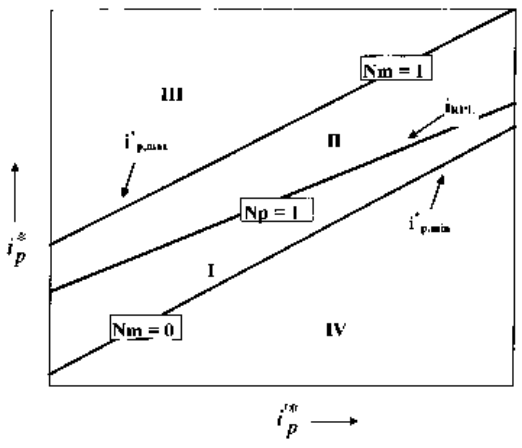

Fig. 4. Schematic illustration of parameter space during reverse-pulse current plating as defined by N_m and N_p.

Table 1. Parameter space for reverse pulse plating

Regions	N_m	N_p	*Theoretical current efficiency* ε
I	< 1	< 1	100
II	< 1	> 1	$0 < \varepsilon < 100$
III	> 1	> 1	$0 < \varepsilon < 100$
IV	< 0	< 1	$\varepsilon < 0$

the results for pulse plating: (i) copper deposits at 100% current efficiency for the condition where N_m and N_p are both less than 1, and (ii) transient diffusion limitations are exceeded before steady-state mass transfer limitations which lowers current efficiency to below 100%.

3. Experimental details

3.1. *Apparatus and procedure*

Copper was plated on a rotating cylinder cathode from a $CuSO_4$–H_2SO_4 electrolyte. The concentration of copper sulfate was either 0.05 or 0.1 M and the content of sulfuric acid was maintained at 1.0 M. The cathode was a 0.8 mm diameter gold plated stainless steel cylinder which was rotated at 1000 rpm in all experiments. The anode was a copper foil placed concentrically at a distance of 45 mm from the cathode. It was found that copper plated by reverse-pulse currents is not adherent to gold. In order to overcome this problem, a 0.5 mm thick copper layer was plated on top of the gold by direct current. The instrumentation for current supply and potential measurement has been described elsewhere [5].

In all reverse-pulse current plating experiments the cathode was mounted on the rotating shaft, immersed in the solution and set at a rotation speed of 1000 rpm. Plating was carried out until a total charge of 6 C was passed, which corresponded to a deposit thickness of 2 μm. Potential transients at the cathode were monitored to detect surface roughening or hydrogen evolution. At the end of each experiment the cathode was washed and dried. Gravimetric measurements were carried out to determine the current efficiency during metal plating. A thin film X-ray fluorescence measurement was carried out to determine the deposit thickness as a cross-check for the gravimetric measurements. Scanning electron microscopy was performed to determine the deposit microstructure. a few deposition experiments with d.c. and pulse-current were also carried out to directly compare the deposit microstructure obtained by the three different plating methods.

3.2. *Choice of pulse parameters*

The diffusion coefficient for the Cu^{2+} species in the 0.05 M and 0.1 M $CuSO_4$ solutions is listed in Table 2. The kinematic viscosity of both electrolytes is

Table 2. Physicochemical properties of electrolytes and pulse parameters

	0.05 M $CuSO_4$/ 1.0 M H_2SO_4	*0.1 M $CuSO_4$ 1.0 M H_2SO_4*
D	6.1×10^{-10} m^2 s^{-1}	5.3×10^{-10} m^2 s^{-1}
i_L	230 A m^{-2}	423 A m^{-2}
δ	2.55×10^{-5} m	2.43×10^{-5} m
T^*	0.0187	0.0179

1.1×10^{-6} m^2 s^{-1}. The rotation speed of the cylinder was set at 1000 rpm for all experiments in order to ensure that the fluid flow was always turbulent and Equation 4 was applicable. The steady-state limiting current, as computed from Equation 4, and the corresponding diffusion layer thickness are also listed in Table 2.

To achieve high instantaneous peak currents, duty cycles of 0.2 and 0.5 were chosen. The pulse period was set at 20 ms which corresponded to an on-time of 4 ms and 10 ms for the 0.2 and 0.5 duty cycles, respectively. The dimensionless pulse time, T^*, corresponding to this pulse period is listed in Table 2 for the two different electrolytes. The value of $i^*_{p,\max}$ was varied between 0.2 and 2.7 times i^*_{RPL} and i'^*_p was set at either 0.5, 1.0, or 2. This choice of pulse parameters enabled the investigation of deposit microstructure for N_m ranging between 0.1 and 1.3, and N_p ranging between 0.1 and 2.2

4. Results

A typical scanning electron micrograph for pulse-plating experiments with N_m and N_p values of less than 1.0 is shown in Fig. 5. As seen in the SEM, deposits were compact and granular and bright to the naked eye. They were well adherent to the copper substrate. When the $CuSO_4$ content in the electrolyte was raised to 0.1 M and the duty-cycle was changed to 0.5, the microstructure was found to be unchanged. Microstructure of deposits obtained by direct-current plating for the same N_m value were found to be similar to those shown in Fig. 5. These results indicate that under the same steady-state mass transfer conditions d.c. and pulse plating of copper yield the same microstructure.

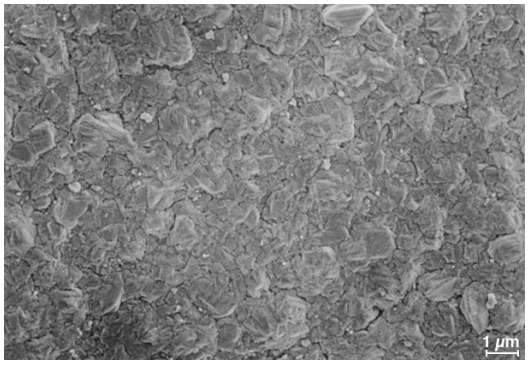

Fig. 5. Microstructure of deposits obtained by pulse-current plating for a 0.05 M $CuSO_4$ and 1.0 M H_2SO_4 solution. Values of N_m and N_p are 0.2 and 0.28.

Unlike d.c. and pulse plating, the deposit is powdery for N_m values between 0.1 and 0.3. The microstructure could not be determined for $N_m = 0.1$, since almost no metal was deposited in any of these experiments. However, metallic powder was detected at the bottom of the cathode at the end of an experiment, showing that Cu^{2+} reduction occurred but Cu powder was not adherent.

Typical structure of copper deposits for $N_m = 0.2$ and 0.3 are presented in Fig. 6. The structure of grains in the deposit, as can be seen from the SEM in the figure, is different from those obtained by using pulse currents. The grains are oblong in shape and separate crystallites are clearly visible. An increase in the reverse current or reverse time encourages the growth of large, separate crystallites and causes the structure to become more oblong (cf. Fig. 6(c)–(e)). The cause for an oblong shape could be due to deposition and dissolution occurring preferentially in different planes. Although current efficiency is expected to be 100% in this regime, it was found to range between 70 and 90%, presumably due to poor adherence.

SEM for higher values of N_m, approximately between 0.4 and 0.6, and N_p close to 1.0 are shown in Fig. 7(a)–(f). The deposit is more compact (cf. Fig. 7(a)–(c),(e)) although the structure is significantly different from that of those obtained by d.c. and pulse plating. The domain of N_m where compact deposits are obtained diminishes when the reverse current is raised: for $i'^*_p = 0.5$ the deposit is compact for N_m between 0.4 to 0.6, whereas for $i'^*_p = 1.0$ it is found only for $N_m = 0.6$. In fact, when the dimensionless reverse-current is raised to 2.0, compact deposits were never obtained. A more columnar growth is observed for N_m values ≥ 0.7. This is due to transient mass-transfer limitations since N_p is very close to 1.0 in these experiments. Current efficiencies were found to range between 93 and 100% as is expected from theoretical considerations.

Columnar or dendritic deposits were obtained whenever N_p or N_m exceeded 1.0, that is, regions II and III in Fig. 4. The transition from granular to dendritic growth is gradual, as has been found for the case of pulse plating [11]. The grains changed from columnar structures, to columns with small arms, followed by fully dendritic growth. Although current efficiencies are expected to be lower than 100% due to competitive hydrogen reduction, the large increase in surface roughness brought about by the dendrites led to a lowering in current density whereby current efficiencies close to 100% were maintained.

Potential transients during reverse-pulse-current plating experiments were of three different kinds which are shown in Fig. 8(a)–(c). Potential transients of type 8a were observed when the values of N_p and N_m were below 1.0, that is, in region I of Fig. 4 for both powdery and compact deposits. The cathode potential during the on time corresponds to copper

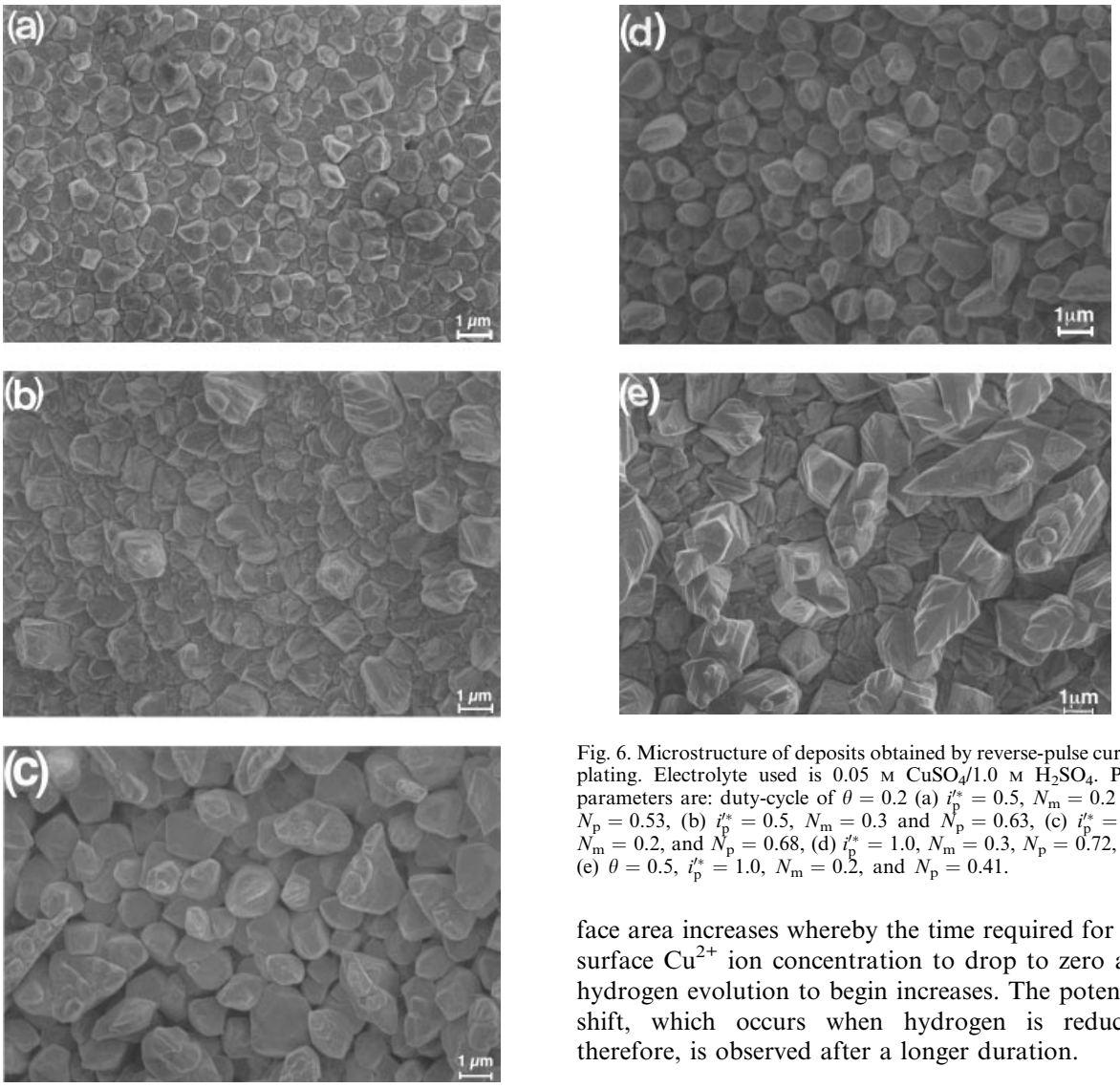

Fig. 6. Microstructure of deposits obtained by reverse-pulse current plating. Electrolyte used is 0.05 M $CuSO_4$/1.0 M H_2SO_4. Pulse parameters are: duty-cycle of $\theta = 0.2$ (a) $i_p'^* = 0.5$, $N_m = 0.2$ and $N_p = 0.53$, (b) $i_p'^* = 0.5$, $N_m = 0.3$ and $N_p = 0.63$, (c) $i_p'^* = 1.0$, $N_m = 0.2$, and $N_p = 0.68$, (d) $i_p'^* = 1.0$, $N_m = 0.3$, $N_p = 0.72$, and (e) $\theta = 0.5$, $i_p'^* = 1.0$, $N_m = 0.2$, and $N_p = 0.41$.

reduction and during the reverse time it increases to that for copper dissolution. In these experiments the shape of the potential transient remained the same for the entire duration of the experiment.

Potential transients of the type shown in Fig. 8(b) were observed when the value of N_p was equal to or just exceeded 1.0 but N_m was less than 1.0, that is, region II. In these experiments, immediately after commencement of plating, there is a clear shift in cathode potential from Cu deposition to hydrogen reduction during the on-time. As plating continues, the potential shift towards hydrogen evolution disappears due to increase in surface roughness. This results in a decrease in the current density to values below i_{RPL} and hydrogen reduction is effectively stopped.

Potential transients of the type shown in Fig. 8(c) were observed when N_p and N_m exceeded 1.0 and the deposit microstructure was clearly dendritic. In this case there is a clear shift in the cathode potential from Cu deposition to hydrogen evolution throughout the plating experiment, although the time required for this shift to occur increases with the duration of metal deposition. As the metal continues to plate, the surface area increases whereby the time required for the surface Cu^{2+} ion concentration to drop to zero and hydrogen evolution to begin increases. The potential shift, which occurs when hydrogen is reduced, therefore, is observed after a longer duration.

5. Discussion

Both theoretical analysis and deposit microstructure show clearly that reverse-pulse current plating can be advantageously carried out within a narrow range of pulse parameters. A dimensionless reverse pulse current up to 2.0 and a pulse period in the range of 1 to 1000 ms is the practical domain of choice when duty cycles of 0.2 or 0.5 are used. Although experiments for reverse-current plating of copper from acid sulfate baths for $i_p'^*$ as high as 10 to 50 have been reported [14], a closer inspection of that article by the present authors reveals that only overall dissolution is possible under those plating conditions.

The powdery deposits obtained for low values of N_m with reverse pulse plating are attributed to the rapid dissolution of newly formed nuclei during the off-time. Andersen *et al.* [15] have performed scanning tunnelling microscopy for both pulse and reverse-pulse current plating. They found that the application of a high cathodic pulse covers the surface with small crystallites in both plating methods, but small copper crystals are dissolved at potentials cathodic to the Cu reversible potential in the latter case. It may be possible that out of the numerous

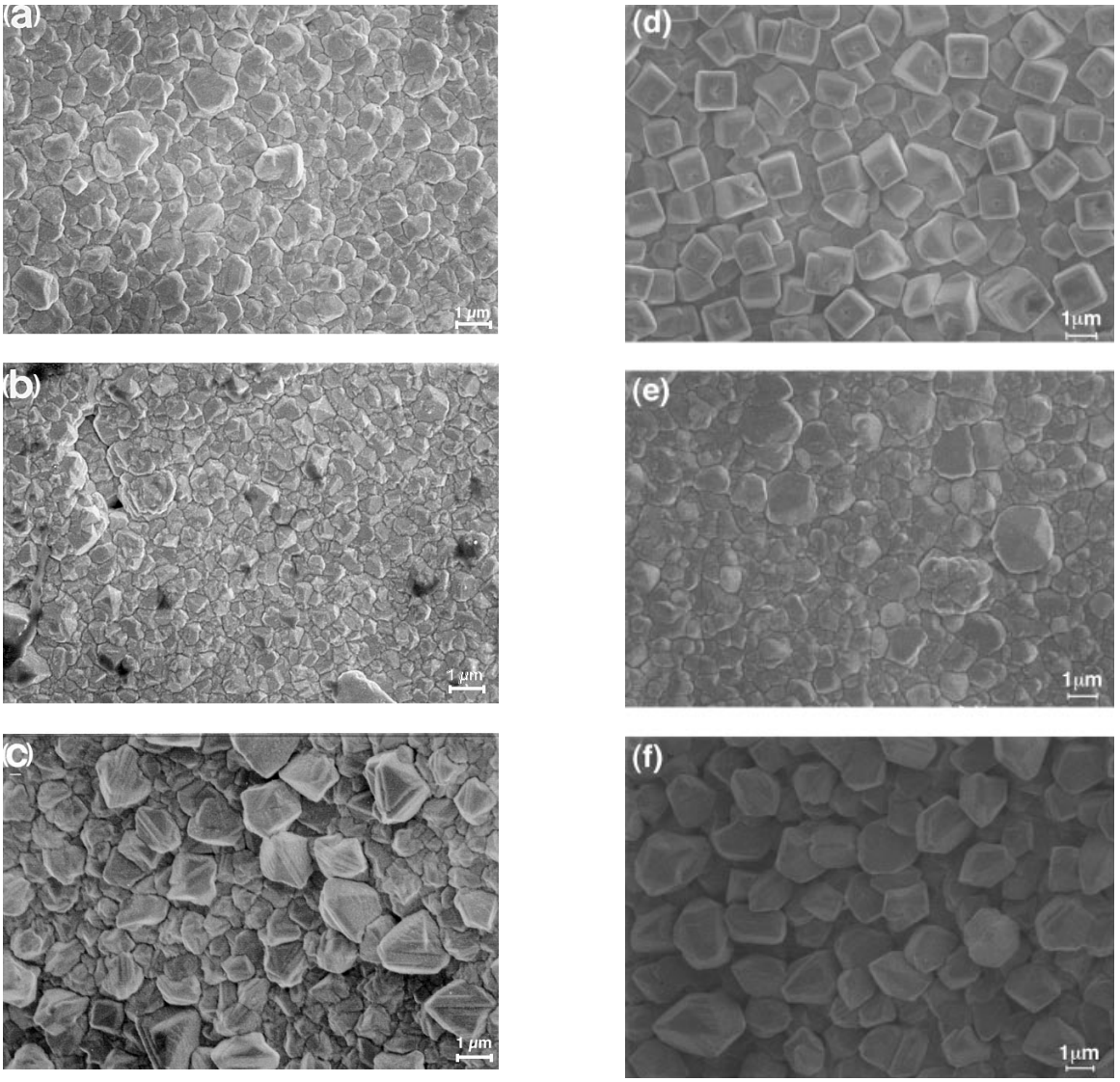

Fig. 7. Deposit microstructure for reverse-pulse current plating from a solution containing 0.05 M $CuSO_4$ and 1.0 M H_2SO_4. Pulse parameters: $\theta = 0.2$, (a–c) $i_p'^* = 0.5$, and (a) $N_m = 0.4$, $N_p = 0.71$, (b) $N_m = 0.6$, $N_p = 0.92$ and (c) $N_m = 0.7$, $N_p = 1.0$. For (d–f) $i_p'^* = 1.0$ and (d) $N_m = 0.4$, $N_p = 0.83$, (e) $N_m = 0.6$, $N_p = 0.97$, and (f) $N_m = 0.7$, $N_p = 1.13$.

nuclei of metallic copper generated during the on-time, only larger crystallites continue to grow. The smaller and less stable crystallites, which have a high energy of formation, are dissolved almost instantaneously during current reversal. As the peak current is raised or the on time lengthened, larger and more stable crystallites are formed which lead to more compact deposits. On the other hand, raising the reverse current results in the complete dissolution of small crystallites and only larger crystals continue to grow, as was also found in this study.

The microstructure of copper deposits obtained by reverse-pulse current plating depends on the parameters N_m and N_p in a less straight forward fashion than for pulse current-plating. In the latter case compact deposits are obtained when both N_p and N_m are smaller than 1, while dendritic deposits are produced for either N_m and N_p exceeding 1. Similarly, during reverse current pulse-plating dendritic deposits were observed whenever N_p or N_m were greater than 1. Contrary to the behaviour in pulse plating, reverse-pulse current plating can lead to loose powdery deposits even in the absence of mass transfer limitations, that is, for N_m and $N_p < 1$. This observation (which needs further investigation) narrows the usable range of parameters during reverse pulse plating. In this study compact deposits were obtained only for $N_m = 0.4$ to 0.6 and $N_p < 1$.

6. Conclusions

A theoretical analysis based on charge-balance and steady-state and transient mass transfer considerations has been used to determine the practical range of parameters during reverse-pulse current plating. The analysis clearly shows that small duty cycles, that is, < 0.5 are necessary in order to achieve high instantaneous peak currents. Pulse periods in the range of 1 to 1000 ms and a dimensionless reverse current up to 2.0 define the practical regime for copper

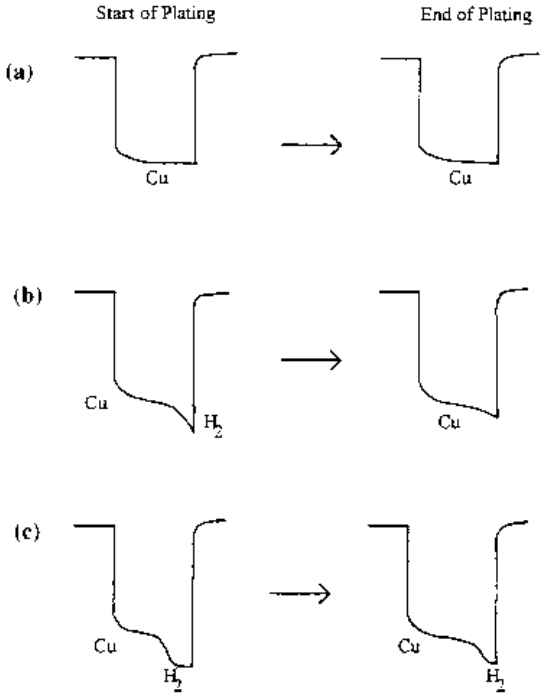

Fig. 8. Potential transients during pulse plating; (a) region I, (b) region II, and (c) region III as defined in Fig. 4.

plating. For pulse times attainable in practice, transient mass-transfer limitations are usually exceeded before those imposed by steady-state diffusion limitations.

The parameter space for reverse-pulse current plating has been defined in terms of steady-state and transient mass transfer parameters, N_m and N_p, respectively. The plating current efficiency is 100% only for the case N_p and N_m are both < 1 and this falls below 100% if N_p exceeds 1. The microstructure of copper deposits obtained by reverse-pulse current plating are powdery for N_m values between 0.1 and 0.3. Compact deposits are obtained for N_m values varying between 0.4 and 0.6 for $i_p'^* = 0.5$, but when the dimensionless reverse current is raised to 2.0 compact deposits are never observed. Noncompact, columnar or dendritic deposits are obtained when either N_p or N_m exceeded 1.0.

Acknowledgements

The authors are grateful to P. Mettraux for carrying out scanning electron micrography. This project was supported by the Fonds National Suisse de la Récherche Scientifique, Berne, Switzerland. Dr S. Roy would like to thank The Department of Chemical and Process Engineering, University of Newcastle upon Tyne, for providing travel expenses.

References

[1] S. S. Kruglikov, M. M. Yarlikov and T. E. Yurchuk, *Electrokhimiya* **27** (1991) 298.
[2] D. T. Chin and M. K. Sunkara, *Plat. Surf. Finish.* **78**(8) (1991) 57.
[3] D. L. Grimmett, M. Schwartz and K. Nobe, *J. Electrochem. Soc.* **139** (1992) 3414.
[4] P. Leisner, G. Bech-Neilsen and Per Møller, Proceedings of AESF Conference (1992) p.1011.
[5] S. Roy, M. Matlosz and D. Landolt, *J. Electrochem. Soc.* **141** (1992) 1509.
[6] D. T. Chin, N. R. K. Vilambi and M. K. Sunkara, *Plat. Surf. Finish.* **76** (1989) 74.
[7] P. Leisner, G. Bech-Neilsen and Per Møller, *J. Appl. Electrochem.* **23** (1993) 1232.
[8] R. D. Grimm and D. Landolt, *Surf. Coat. Technol.* **31** (1987) 151.
[9] P. Leisner, Thesis: PI 92.24-A. AP92.39, The Technical University of Denmark (1992).
[10] P. Leisner, D. Ulrich and Per Møller, *Plat. Surf. Finish.* **79**(7) (1992) 62.
[11] O. Chène and D. Landolt, *J. Appl. Electrochem.* **19** (1989) 188.
[12] H. Y. Cheh, *J. Electrochem. Soc.* **118** (1971) 1132.
[13] M. Eisenberg, C. W. Tobias, and C. R. Wilke, *ibid.* **101** (1954) 307.
[14] J. Y. Wang, D. Balamurugan, and D. T. Chin, *J. Appl. Electrochem.* **22** (1992) 240.
[15] J. E. T. Andersen, G. Bech-Neilsen and Per Møller, *Surf. Coatings Technol.* **67** (1994) 151.
[16] D. T. Chin, *J. Electrochem. Soc.* **130** (1983) 1657.
[17] M. Abramowitz and I. A. Stegun (Eds) 'Handbook of Mathematical Functions' 9th edn, Dover Publications, New York (1972) p 808.

Appendix

Mathematical expressions for reverse-pulse limiting currents have been derived by Cheh [12] and Chin [14, 16]. Whereas Cheh obtained a limiting current expression for the specific case of reverse-current plating, Chin derived an expression for a general pulse form from which the value of i_{RPL} can be calculated. At first sight the equations derived by these two researchers appear to be different but as shown below, they are, in fact, equal.

The reverse-pulse current equation derived by Cheh [12] is

$$\frac{i_{RPL}}{i_L} = \frac{1.0}{1.0 - \frac{8}{\pi^2}\left(1 + \frac{i_p'}{i_{RPL}}\right)\sum_{m=1}^{\infty}\frac{1}{(2m-1)^2}\frac{\exp\left[(2m-1)^2 a\, t_{rev}\right]-1}{\exp\left[(2m-1)^2 a\, T\right]-1}} \tag{A1}$$

where $a = \pi^2 D/4\delta^2$. In this paper we have used a positive sign convention for both cathodic and anodic currents whereby a summation is used in the bracketed term $(1 + i_p'/i_{RPL})$. Equation A1 is rewritten by normalizing i_p' and i_{RPL} with respect to i_L:

$$i^*_{RPL} = \frac{1.0}{1.0 - \frac{8}{\pi^2}\left(1 + \frac{i_p'^*}{i^*_{RPL}}\right)\sum_{m=1}^{\infty}\frac{1}{(2m-1)^2}\frac{\exp\left[(2m-1)^2 a\, T(1-\theta)\right]-1}{\exp\left[(2m-1)^2 a\, T\right]-1}} \tag{A2}$$

When the dimensionless reverse limiting current is brought to the left-hand side of the equation we obtain

$$i^*_{RPL} = \frac{1.0 + \frac{8}{\pi^2} i_p'^* \sum_{m=1}^{\infty}\frac{1}{(2m-1)^2}\frac{\exp\left[(2m-1)^2 a\, T(1-\theta)\right]-1}{\exp\left[(2m-1)^2 a\, T\right]-1}}{1.0 - \frac{8}{\pi^2}\sum_{m=1}^{\infty}\frac{1}{(2m-1)^2}\frac{\exp\left[(2m-1)^2 a\, T(1-\theta)\right]-1}{\exp\left[(2m-1)^2 a\, T\right]-1}} \tag{A3}$$

The numerator on the right hand side of Equation A3 can be rewritten in a simpler form by replacing the variables with λ_m and T^*

$$1.0 + 2i'^*_p T^* \sum_{m=1}^{\infty} \frac{\exp[\lambda_m(1-\theta)] - 1}{\lambda_m[\exp[\lambda_m] - 1]} \tag{A4}$$

The denominator in the right hand term of Equation A3 is also rewritten in terms of λ_m and T^*

$$1.0 - 2T^* \sum_{m=1}^{\infty} \frac{\exp(\lambda_m(1-\theta)) - 1}{\lambda_m[\exp(\lambda_m) - 1]} \tag{A5}$$

The limiting reverse-pulse current equation, obtained from Equation A3–A5, is then

$$i^*_{RPL} = \frac{1.0 + 2i'^*_p T^* \sum_{m=1}^{\infty} \frac{\exp(\lambda_m(1-\theta))-1}{\lambda_m[\exp(\lambda_m)-1]}}{1.0 - 2T^* \sum_{m=1}^{\infty} \frac{\exp(\lambda_m(1-\theta))-1}{\lambda_m[\exp(\lambda_m)-1]}} \tag{A6}$$

The reverse-pulse limiting current, as derived by Chin [13, 16], is

$$i^*_{RPL} = \frac{1.0 + 2i'^*_p T^* \sum_{m=1}^{\infty} \frac{\exp(-\lambda_m\theta)-\exp(-\lambda_m)}{\lambda_m[1-\exp(-\lambda_m)]}}{2T^* \sum_{m=1}^{\infty} \frac{1-\exp(-\lambda_m\theta)}{\lambda_m[1-\exp(-\lambda_m)]}} \tag{A7}$$

The numerator on the right hand side of Equation A7 can be rewritten by multiplying and dividing the series summation term by exp (λ_m)

$$1.0 + 2i'^*_p T^* \sum_{m=1}^{\infty} \frac{\exp[\lambda_m(1-\theta)] - 1}{\lambda_m[\exp\lambda_m - 1]} \tag{A8}$$

The denominator on the right hand side of Equation A7 is rearranged by multiplying and dividing the summation term with exp (λ_m)

$$2T^* \sum_{m=1}^{\infty} \frac{\exp\lambda_m - \exp\lambda_m(1-\theta)}{\lambda_m[\exp\lambda_m - 1]} \tag{A9}$$

The expression in Equation A9 is split up into two series of summation terms by adding and subtracting unity in the numerator to obtain,

$$2T^* \sum_{m=1}^{\infty} \frac{1}{\lambda_m} - 2T^* \sum_{m=1}^{\infty} \frac{[\exp(\lambda_m(1-\theta)) - 1]}{\lambda_m[\exp\lambda_m - 1]} \tag{A10}$$

The sum of the first series in Equation A10,

$$2T^* \sum_{m=1}^{\infty} \frac{1}{\lambda_m}$$

as obtained by replacing λ_m with $\pi^2 T^*$ (m - 1/2)^2 is

$$\frac{8}{\pi^2} \sum_{m=1}^{\infty} \frac{1}{(2m-1)^2}$$

The value of

$$\sum_{m=1}^{\infty} \frac{1}{(2m-1)^2}$$

is exactly equal to $\pi^2/8$ [17]; the value of

$$\frac{8}{\pi^2} \sum_{m=1}^{\infty} \frac{1}{(2m-1)^2}$$

therefore, is exactly unity. The equation for reverse-pulse limiting current, therefore, derived using Equations A7 to A10 therefore is

$$i^*_{RPL} = \frac{1.0 + 2i'^*_p T^* \sum_{m=1}^{\infty} \frac{\exp(\lambda_m(1-\theta)) - 1}{\lambda_m[\exp(\lambda_m) - 1]}}{1.0 - 2T^* \sum_{m=1}^{\infty} \frac{\exp(\lambda_m(1-\theta)) - 1}{\lambda_m[\exp(\lambda_m) - 1]}} \tag{A11}$$

which is identical to Equation A6.